A comparison between different approaches for modelling media with viscoelastic properties via optimization analyses

Tomasz Lekszycki[1,2], **Sara Bucci**[2,5,*], **Dionisio Del Vescovo**[2,3], **Emilio Turco**[2,4], **and Nicola Luigi Rizzi**[2,6]

[1] Warsaw University of Technology, Warsaw, Poland
[2] M&MoCS, International Research Center for the Mathematics & Mechanics of Complex Systems, Università dell'Aquila, Italy
[3] Department of Mechanical and Aerospace Engineering, University La Sapienza, Rome, Italy
[4] Dipartimento di Architettura, Design e Urbanistica, Università degli Studi di Sassari, Italy
[5] Institute of Mechanics, Otto-von-Guericke-Universität Magdeburg, Germany
[6] Department of Architecture, University of Roma Tre, Rome, Italy

Key words Viscoelastic materials, solid mechanics, optimization theory, linear elasticity, viscosity.

In this paper we deal with the problem of choosing the best linear model capable to describe the mechanical characteristics and the behavior of media with viscoelastic properties. Two different cases are studied: asphalt concrete subject to forced vibrations and PVC cantilever beam subject to free vibrations. In both cases, experimental results are compared with specific models and the identification of the most suitable one is carried out with the help of optimization theories, namely the minimization of an objective function, the Kalaman filtering or the Bland and Lee approach.

1 Introduction

Motivation and basic ideas

Nowadays, the necessity of having good mechanical models for describing the behaviour of various materials is pressing. Experimental data can be obtained by different laboratory setups, which may test mechanical properties (such as strength, hardness, ductility) under certain specific loading conditions. This could be a good starting point for the characterization of material models; however, it is quite restrictive, since a model obtained in this way, cannot be used when different loading schemes have to be considered. Therefore, a good method, capable of including a wider range of behaviors, is required.

The characterization of a material, in particular in the case of viscoelastic materials, is usually made in two steps: first one chooses the mathematical model and then he evaluates the proper parameters which fit in it. Nevertheless, obtaining the right values for the elements that model our material, i.e. the stiffness of a spring or the viscous damping of a dashpot, is far to be a simple matter. Obviously, when the constitutive relations are known, it is much easier to identify the material constants; still this would be not enough to perform effective analysis, meant to be more accurate with respect to simplified engineering analysis, which may come out too rough to ensure total reliability of the results.

In this paper, we propose a comparison between different models, in order to choose which one can best determine the viscoelastic properties of our materials. Each of these models must be able to describe all the basic mechanical properties and phenomena of the considered material while preserving generality and simplicity e.g. by limiting the number of material parameters (for investigations in similar directions the reader may see e.g. [25, 26, 31, 36, 51]). This will make the model suitable for further applications in complex numerical calculations, for experimental identification and for mechanical interpretation i.e. the identification of the model parameters with specific effective material behaviors. The final choice will be made by confronting the models parameters, found analytically or by FEM analysis, with the ones obtained by laboratory experiments, via different methods taken from optimization theory, namely the least square method, the Kalman filtering and the sensitivity analysis.

It is well known that fractional calculus has proved a reliable tool for the description of visco-elastic phenomena (see for instance [28,39]). The richness and the flexibility provided by fractional calculus is clearly much greater when compared to the models of linear visco-elasticity. However, it is also becoming increasingly common the need of analyzing the behavior

of a very large number of elementary constituents, for instance when dealing with complex microstructures [23]. This means that computation speed has also to be taken into account when comparing the advantages of various models, and in this respect the simplicity of linear models comes in handy. This justifies our choice in the present work.

Two different cases are considered: first, a Polivinilchloride cantilever beam which is clamped at one end and whose free end is subject to an initial displacement and then set free to vibrate; second, a block of Asphalt concrete fixed to an hydraulic system which imposes forced vibrations to the specimen. The two experimental phenomena are clearly of different nature, both concerning the material analysed and the set-up and type of tests which they undergo. In the present paper, however, we want to emphasize the identification method more than the details of the two cases. Explicitly, in both cases we:

- perform experiments on the real material
- extract relevant data from each experiment
- examine and choose different viscoelastic models which can describe the behavior of the considered case
- test the different models with a fitting procedure
- select the best model for the considered case.

The whole procedure is setup at room temperature, therefore thermal effect are neglected, and plasticity effects are excluded. Moreover we restrict for simplicity our analyses to one-dimensional cases.

2 Specimens and experimental setups

As stated in the introduction, in order to be able to select the most suitable model to the considered viscoelastic material, we need to be supported by experimental results. We will try to model a viscoelastic cantilever beam, which can be found in sandwich structures, as core material, and viscoelastic composites, as concrete asphalt.

In this section, we describe both the materials that we are going to consider and the laboratory experiments. The values obtained in this way will be used later on (see Sect. 4) in the objective function, in order to measure the differences between analytical solutions and measured displacements.

We recall once again that we will study different experimental conditions in the two cases (in particular, free versus forced vibrations). Therefore we will obtain clearly different outputs; nevertheless the method summarized at the end of Sect. 1 can be applied in both cases.

2.1 Polivinilchloride cantilever beam

We consider a beam made of Polivinilchloride (PVC) foam. The beam is clamped to a steel frame which is rigidly attached to a concrete basement. The measuring equipment is mounted on the top of the frame and is composed by a laser diode module with an optical focus, a mirror glued to the middle and to the free end of the beam and a light sensitive receiver, which converts the reflected laser beams into the corresponding electrical signal. Every signal is collected by the data processing unit (B & K dual channel analyser) and stored into a computer hard disk. We can see a schematic representation of the experiment in Fig. 1.

In order to register the free vibrations of the beam, we need to impose initial conditions of displacement and velocity to its free end. This will be enforced by a specific rotatable device which is then removed instantaneously at time $t = 0.1$ s. The free vibration curve of the sample is shown in Fig. 2.

It can be immediately observed that the response is not exactly the one of a classical Voigt material model. Actually, it shows aperiodic contributions to the total motion, indicating the presence of material relaxation.

2.2 Asphalt concrete

Laboratory experiments have also been performed on cylindrical samples of asphalt D100 with 15% of rubber flower. The specimen is glued from the end surfaces to two steel fixtures, in a way that all components lie in a coaxial position. An extensometer Denison of the type LVTD was prepared so as to enable measurements of the strain for the whole length of the sample. The hydraulic Instron 1251 machine grips the specimen and assures vibrations at given amplitudes and frequencies. A displacement and force transducer collects the electric signals and, via the Instrom control system, transmits them to the digital oscilloscope (Tektronix 2230) and to the computer (see Fig. 3).

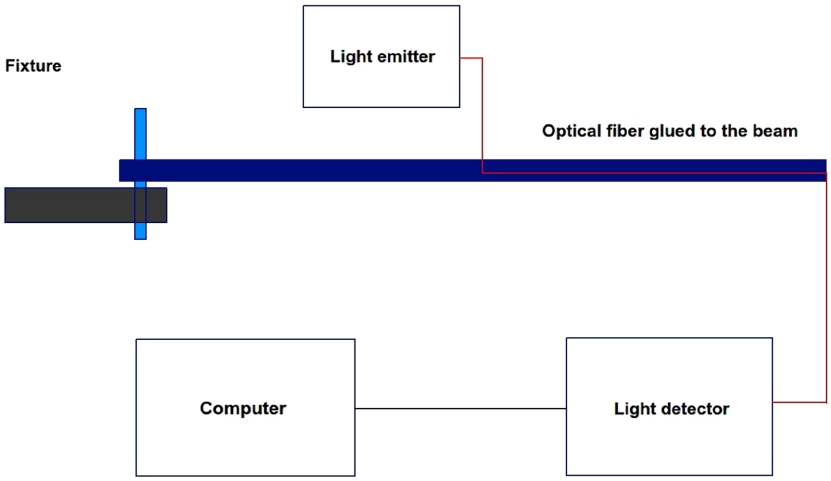

Fig. 1 Schematic representation of the experimental fixture for the free vibration test of the PVC beam.

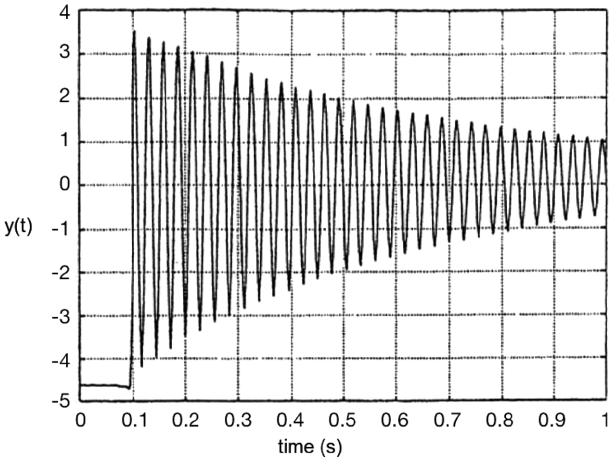

Fig. 2 Free vibration response of the viscoelastic PVC beam.

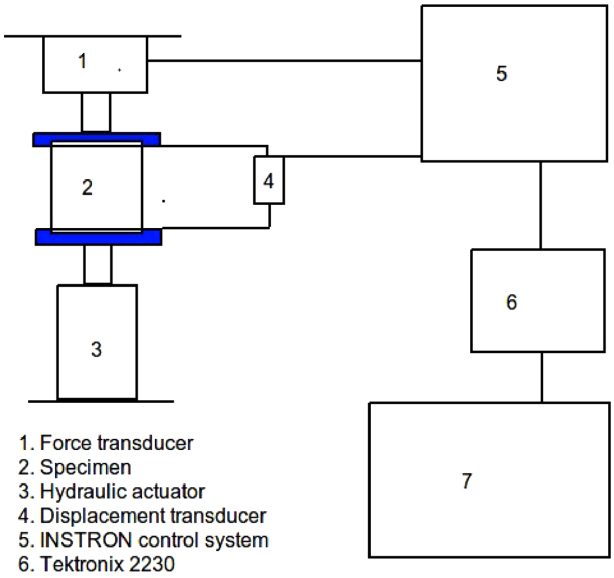

Fig. 3 Schematic representation of the experimental fixture for the vibration test of the Asphalt concrete.

The results for stress $\sigma(t)$ and strain $\epsilon(t)$ are plotted in Fig. (4). As we can see, an approximation of the experimental results can be made in the following way:

$$\begin{aligned} \sigma(t) &= \sigma \sin(\omega t + \alpha) = A_N \sin(\omega t) + B_N \cos(\omega t), \\ \epsilon(t) &= \epsilon \sin(\omega t + \beta) = A_0 \sin(\omega t) + B_0 \cos(\omega t), \end{aligned} \tag{1}$$

where

$$\tan(\alpha) = \frac{B_N}{A_N} \quad \text{and} \quad \tan(\beta) = \frac{B_0}{A_0}$$

and thus the phase shift δ can be calculated using

$$\tan(\delta) = \frac{A_0 B_N - A_N B_0}{A_0 A_N - B_N B_0}. \tag{2}$$

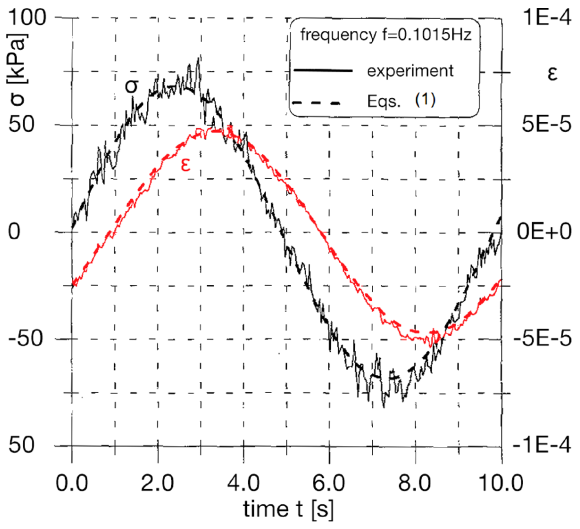

Fig. 4 Strain and stress curves obtained via experimental measurements at frequency f = 0.1015 Hz and, in dashed lines, their approximating functions described by Eqs. (1).

3 Material models

In this section, we are going to analyse models that can describe our materials. These models will be then compared with the previous experimental results.

3.1 PVC Beam

In our model we neglect shear deformations and rotary inertia effect. Moreover, we assume small displacement and slope of the beam (see section on results for possible generalizations of these assumptions). Therefore, the motion of the beam is governed by the classical Euler-Bernoulli equation:

$$\frac{\partial^2 M(x,t)}{\partial x^2} - \rho A \frac{\partial^2 y(x,t)}{\partial t^2} = 0. \tag{3}$$

With the following initial conditions:

$$\begin{cases} y(l,0) = y_0 \approx -4,65 \text{ cm}, \\ v(l,0) = v_0 = 0. \end{cases} \tag{4}$$

As usual, $M(x,t)$ denotes the bending moment of the beam, ρ the mass per unit volume and A the cross-section area (which is constant).

Voigt-Kelvin model

The Voigt-Kelvin material model cam be schematically represented as in the Fig. 5. It is simply composed by a viscous damper with damping constant $p_1 = EI\xi$, in parallel with an elastic spring with stiffness constant $p_0 = EI$. Since such elements are posed in parallel, the stress and strain for each component are the same. The associated constitutive equation is:

$$M(x,t) = -p_0 \frac{\partial^2 y(x,t)}{\partial x^2} - p_1 \frac{\partial}{\partial t} \frac{\partial^2 y(x,t)}{\partial x^2}. \tag{5}$$

If we plug (5) into Eq. (3) we get the initial value problem

$$\begin{cases} p_0 \dfrac{\partial^4 y(x,t)}{\partial x^4} + p_1 \dfrac{\partial}{\partial t} \dfrac{\partial^4 y(x,t)}{\partial x^4} + \rho A \dfrac{\partial^2 y(x,t)}{\partial x^2} = 0, \\ y(l,0) = y_0, \\ v(l,0) = v_0, \end{cases} \tag{6}$$

that is the equation of motion of a classically damped beam in terms of displacement.

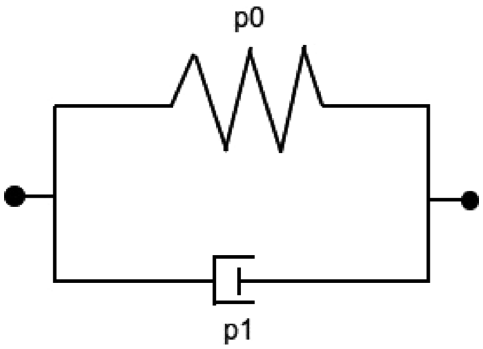

Fig. 5 Schematic representation of the Zener model.

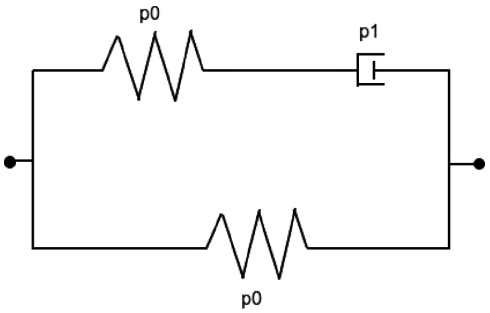

Fig. 6 Schematic representation of the Voigt-Kelvin model.

Zener model

The Zener model is slightly more complex than Voigt's one, since it involves both elements in parallel and elements in series (see Fig. 6). It is also known as standard linear solid model and it requires the use of a third parameter q_1 which stands for the time constant. The constitutive relation reads:

$$M(x,t) + q_1 \frac{\partial M(x,t)}{\partial t} = -p_0 \frac{\partial^2 y(x,t)}{\partial x^2} - p_1 \frac{\partial}{\partial t} \frac{\partial^2 y(x,t)}{\partial x^2}. \tag{7}$$

In the same fashion as we did for the Voigt model, we substitute (7) into (3) and get the Zener three-parameter equation of beam motion with the initial conditions

$$\begin{cases} p_0 \dfrac{\partial^4 y(x,t)}{\partial x^4} + p_1 \dfrac{\partial}{\partial t} \dfrac{\partial^4 y(x,t)}{\partial x^4} + \rho A \dfrac{\partial^2 y(x,t)}{\partial x^2} + \rho A q_1 \dfrac{\partial^3 y(x,t)}{\partial t^3} = 0, \\ y(l,0) = y_0, \\ v(l,0) = v_0, \\ a(l,0) = a_0. \end{cases} \tag{8}$$

The initial acceleration a_0 is found solving the Eq. (3) with initial configuration $\bar{y}(x,0)$ provided by solution of the static linear problem of a cantilever beam with imposed transverse displacement of y_0 at the free end and initial velocity $\dot{\bar{y}}(x,0) = 0$ (see for instance the standard reference [24]).

Solution and finite element model

The solutions of the previous Eqs. (6) and (8) can be approximated as follows:

$$y(x,t) = \sum_{i=1}^{\infty} X_i(x) T_i(t), \tag{9}$$

with

$$X_i(x) = C_1 \sin(\lambda_i x) + C_2 \cos(\lambda_i x) + C_3 \sinh(\lambda_i x) + C_4 \cosh(\lambda_i x). \tag{10}$$

As we can notice, the previous eigenfunctions are equivalent to those of the elastic beam. The integration constants $C_j, \quad j = 1, ..., 4$ depend on the boundary conditions. Finally, the eigenvalues λ_i are the roots of

$$\cos(\lambda_i l) \cosh(\lambda_i l) = 1, \tag{11}$$

characteristic equation, where l is the length of the beam. We determine the functions $T_i(t)$ starting from the Zener model, using the following:

$$\frac{\rho A}{EI} \left\{ q_i \frac{d^3 T_i}{dt^3} + \frac{d^2 T_i}{t^2} \right\} + \lambda_i^4 \left\{ \xi \frac{dT_i}{dt} + T_i \right\} = 0, \qquad i = 1, \ldots, \infty. \tag{12}$$

Recalling that for the elastic beam, the circular eigenvalues are $\omega_i = \lambda_i^2 \sqrt{EI/\rho A}$, we obtain

$$q_i \Omega_i^3 + \Omega_i^2 + \omega_i^2 \xi \Omega_i + \omega_i^2 = 0. \tag{13}$$

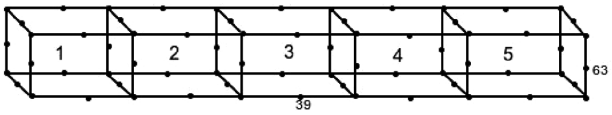

Fig. 7 Finite element model of the viscoelastic cantilever beam.

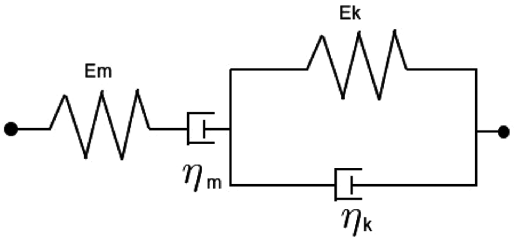

Fig. 8 Schematic representation of Burger's model.

The previous one is the equation for the eigenfrequencies of the three parameter viscoelastic beam of Zener model; it has either three real solutions or one real and two complex conjugates. We are interested in the second case, hence the solutions which associate eigenvalues Ω_i with $X_i(x)$ are

$$\Omega_i^{(1)} = \alpha_i^{(1)}, \quad \Omega_i^{(2)} = \alpha_i^{(2)} + i\omega_{vi}, \quad \Omega_i^{(3)} = \alpha_i^{(2)} - i\omega_{vi}. \tag{14}$$

Therefore, we can express (13) as

$$T_i^v(t) = A_i e^{\alpha_i^{(1)}} + e^{\alpha_i^{(2)} t} \left\{ B_i \sin(\omega_{vi} t) + C_i \cos(\omega_{vi} t) \right\}. \tag{15}$$

In order to obtain the solution for the Voigt material, is sufficient to notice that the first term of Eq. (15) is zero, yielding thus to the classical motion for the damped beam:

$$T_i^v(t) = e^{\alpha_i t} \left\{ B_i \sin(\omega_{vi} t) + C_i \cos(\omega_{vi} t) \right\}. \tag{16}$$

In both cases, we can determine the constants A_i, B_i, C_i from the initial conditions given by Eq. (9) by imposing a kinematic displacement at the free end, $y_0(l)$, and assuming the velocity at time instant $t = 0.1$ s to be equal zero.

To conclude the study of the models for the viscoelastic beam we have to make some remarks: although we found simple analytical models for our material, these may present strong limitations. In particular, the response of the beam modelled in that way does show neither shear deformations (which may result important for many applications) nor rotary inertia effects. We can overcome these problems creating a linear finite element of the beam. As we can see from the Fig. 7 the model is composed of 5 isotropic brick elements, with 20 nodes each, for a total of 180 active degrees of freedom.

With the help of the finite element model we are able to better represent the physical and geometric properties of the beam. Moreover, the equations obtained in this way are directly applicable for the Kalman filtering, as we will see in Sect. 4.2.

As in the standard FE analysis the equation of motion of the beam reads:

$$\mathbf{M}\ddot{u} + \mathbf{C}\dot{u} + \mathbf{K}u = f(t), \tag{17}$$

with $\mathbf{M}$ being the mass, $\mathbf{C}$ the damping, and $\mathbf{K}$ the stiffness matrices; u is the vector of unknown displacements and $f(t)$ a deterministic excitation vector. In the case of Voigt 2-parameter model, since the damping and stiffness parameteres are the same for each element, we can write Eq. (17) as follows:

$$\mathbf{M}\ddot{u} + p_1\mathbf{C}'\dot{u} + p_0\mathbf{K}'u = f(t), \tag{18}$$

where p_0 and p_1 are the identified stiffness and damping parameters. Concerning the Zener model, since we cannot directly use Eq. (18), we need a different type of finite element. Therefore, in order to identify material parameters, we use the approximate analytical solution (9).

3.2 Asphalt concrete

Let us consider isotropic viscoelastic material, one-dimensional case. The general linear constitutive relation can be introduced as follows:

$$p_0\sigma(t) + p_1\frac{d\sigma(t)}{dt} + p_2\frac{d^2\sigma(t)}{dt^2} + \ldots = q_0\epsilon(t) + q_1\frac{d\epsilon(t)}{dt} + q_2\frac{d^2\epsilon(t)}{dt^2} + \ldots \quad . \tag{19}$$

The above formula can be written in a compacted way as

$$P(D)\sigma(t) = Q(D)\epsilon(t), \tag{20}$$

where

$$P(D) = \sum_{k=0}^{M} p_k D^k, \qquad Q(D) = \sum_{k=0}^{N} q_k D^k \qquad k \in \mathbb{N} \tag{21}$$

are linear differential operators and $D^k = \frac{d^k}{d^k t}$ is the differentiation with respect to time; as usual $\sigma(t)$ and $\epsilon(t)$ are respectively the stress and strain fields, while p_k, q_k are the constant parameters.

Burger's model

Let us consider one of the simplest way of using formula (19), which is by means of Burgers model. This model, schematically represented in Fig. 8, is composed by two dampers, with viscous damping parameters η_k, η_M, and two springs, with relatively stiffness parameters E_k, E_M. We can thus write the associated equation in the following form:

$$\sigma + A\frac{d\sigma}{dt} + B\frac{d^2\sigma}{dt^2} = C\frac{d\epsilon}{dt} + D\frac{d^2\epsilon}{dt^2}. \tag{22}$$

We can write the constants A, B, C, D in terms of the material parameters

$$A = \frac{\eta_M}{E_M} + \frac{\eta_M}{E_k} + \frac{\eta_k}{E_k}, \qquad B = \frac{\eta_M \eta_k}{E_k E_M}, \qquad C = \eta_M, \qquad D = \frac{\eta_M \eta_k}{E_k}. \tag{23}$$

If we consider a steady harmonical vibration, we can express the time dependence of stress and strain with the complex relations

$$\begin{aligned} \sigma(t) &= \sigma e^{i\omega t} = (\sigma^R + i\sigma^I)(\cos(\omega t) + i\sin(\omega t)) \\ &= (\sigma^R \cos(\omega t) - \sigma^I \sin(\omega t)) + i(\sigma^R \sin(\omega t) + \sigma^I \cos(\omega t)), \end{aligned} \tag{24}$$

$$\begin{aligned} \epsilon(t) &= \epsilon e^{i\epsilon t} = (\epsilon^R + i\epsilon^I)(\cos(\epsilon t) + i\sin(\epsilon t)) \\ &= (\epsilon^R \cos(\epsilon t) - \epsilon^I \sin(\epsilon t)) + i(\epsilon^R \sin(\epsilon t) + \epsilon^I \cos(\epsilon t)) \end{aligned} \tag{25}$$

where ω is the vibraiton frequency, expressed in rad/s, and σ and ϵ stand for the stress and strain complex amplitudes, independent of time. We can use the previous formulas in order to get rid of the time dependence of the constitutive relation and write them in the complex form. Indeed, if we plug expressions (24) and (25) in (20), deriving and simplifying we arrive to

$$\sigma = E^*(\omega)\epsilon, \tag{26}$$

with E^* denoting the complex stiffness parameter, which could be compared to a stiffness or shear modulus of linear elasticity.

This relation describes the connection between stress and strain relatives amplitudes, also including the shift between their phases, considering various values for the frequencies of vibrations; for this reason, it is often used for investigating the dynamic properties of viscoelastic materials, mechanically represented by different combinations of elastic springs and viscous dashpots.

Notice that a substantial improvement of the numerical model could be obtained by using B-spline or NURBS interpolations (NURBS are a generalization useful to represent exactly circles and ellipses). A simple introduction to NURBS regarding 1-D beams, and the related problems, is reported in [8, 9, 13, 29, 30] while for fully 3-D B-spline isoparametric finite elements see [5]. Moreover dynamic problems could also be explored by using refined 1-D numerical models such as presented in [10, 11].

4 Optimization techniques

Up to now, we just described our experimental setups and results and different material models which may fit to the viscoelastic bodies subject of this study. The identification problem comes when one has to describe the real material, with enough accuracy, for given ranges of initial excitations; In order to select the most suitable differential model, that makes use of independent of initial conditions constants, we have to be able to select the adequate number of material parameters necessary to describe the behaviour of the body. This is done through the use of an objective function, which is usually a mean for measuring the difference between experimentally assessed and analytically calculated response of a material.

4.1 Least square method

The first method that we will see, is the most straightforward, and is easily applicable to the Zener material model (see Sect. 3). As we saw from the experimental setup (see Sect. 2.1) the displacements of nodes 39 and 63, that are respectively at the middle and at the free end of the beams, are measured in a discrete set t_i $(i = 0, ..., N)$ of instants, in both x and y directions (see Fig. 7). We can write the objective function $F(\theta)$, taking the analytical solution of Eq. (9), in its own form, and comparing it with the measured one, as follows:

$$F(\theta) = \sum_{i=0}^{N} \left\{ \bar{y}_i(x) - z(x, t_i) \right\}^2, \tag{27}$$

where $\bar{y}_i(x) = \frac{1}{t_{i+1} - t_i} \int_{t_i}^{t_{i+1}} y(x, t) dt$ is the mean value of the theoretical solution in the i-th time step, $z(x, t_i)$ are the measured displacements and θ is a vector of unknown material parameters. As we minimize the previous objective function, we get the set of equations:

$$\frac{\partial F}{\partial \theta_i} = \sum_{i=1}^{N} 2 \left\{ \bar{y}(x) - z(x, t_i) \right\} \frac{\partial \bar{y}(x)}{\partial \theta_j} = 0, \qquad j = 1, ..., n \tag{28}$$

where n represents the number of material parameters. It should be clear that, using the previous equation and if more oscillations have to be considered, computations may become harder. Fortunately, theoretical analysis has shown that, in the response of a cantilever beam subject to an initial displacement at its free end, only the first two mods can be observed and only one of them is predominant (see for example [34–36]). This is also confirmed by the spectral analysis of the beam response, as we will see in the next Sect. 5.

4.2 Kalman filter

The next method we are going to explain will be able to evaluate the parameters recursively as they are part of a state vector. It will be then applied to the Voigt material model. The advantage of using Kalman algorithm is that it is able to filter noisy and biased measurements, producing estimates of the unknown parameters.

As we will see, the filter is mainly divided in two steps: in the first one the values of the current state variables are predicted, though with their errors; in the second one, after obtaining the next measurement, the values are updated, using a weighted average, giving more importance to the more accurate estimates. As new measurements are observed the algorithm is repeated.

In our paper we are not going to use the classical Kalman filter but rather a generalization of it which works with nonlinear systems, namely, the extended Kalman filter.

Consider the measurements $z(t)$ and the state variables $y(t)$. The relationship between the two in the Kalman filtering algorithm is:

$$\begin{Bmatrix} z(t) \\ \dot{z}(t) \end{Bmatrix} = \mathbf{T} \begin{Bmatrix} y(t) \\ \dot{y}(t) \end{Bmatrix} + \mathbf{W}(t), \tag{29}$$

where $\mathbf{W}(t)$ is a vector whose components are uncorrelated zero mean white noise, and $\mathbf{T}$ is a linear transformation matrix, that in our case reduces to the identity matrix due to the fact that we directly measure the displacements of the corresponding nodes. As regarding the velocities, which are not directly measured, we could reconstruct them from the displacements, by numerical differentiation or apply direct Fourier transform. In this way, excessive vibration modes will be directly filtered, useless since they do not bring any information on the estimated parameters. After adding the parameter vector θ to the state vector, $y^T = \left\{ u^T, \dot{u}^T, \theta^T \right\}$, and introducing $H(t) = (C'\dot{u} \quad K'u)$ and $h(t) = p_1 C'\dot{u} + p_0 K'u$, we can rewrite Eq. (29) in the state space form as follows:

$$\begin{pmatrix} C & M & 0 \\ M & 0 & 0 \\ 0 & 0 & I \end{pmatrix} \dot{y} - \begin{pmatrix} -K & 0 & -H(t) \\ 0 & M & 0 \\ 0 & 0 & 0 \end{pmatrix} y = \begin{pmatrix} f(t) \\ 0 \\ 0 \end{pmatrix} + \begin{pmatrix} h(t) \\ 0 \\ 0 \end{pmatrix} + \begin{pmatrix} 0 \\ 0 \\ w(t) \end{pmatrix}. \tag{30}$$

Last equation can also be reformulated in the shorter form:

$$\mathbf{A}\dot{x} - \mathbf{B}x = c(t) + d(t) + e(t). \tag{31}$$

Taking its expectation we can arrive to the *prediction of the mean* by the equation:

$$\mathbf{A}\widehat{\dot{x}} - \mathbf{B}'\widehat{x} = c(t) \quad \text{where} \quad \mathbf{B}' = \begin{pmatrix} -K & 0 & 0 \\ 0 & M & 0 \\ 0 & 0 & 0 \end{pmatrix}, \tag{32}$$

whose corresponding eigenvalue problem is

$$\mathbf{A}\Phi\Lambda - \mathbf{B}'\Phi = 0 \tag{33}$$

being Λ the vector of eigenvalues and Φ the modal matrix. If we use the transformation $\widehat{x} = \Phi\widehat{z}$ to decouple Eq. (33) and represent it in the modal coordinates z, we can find the analytical solution, which reads:

$$\widehat{z}_k(t) = \mathrm{e}^{\lambda_k(t-t_0)} \left\{ \widehat{z}_k(t_0) + \int_0^{t-t_0} p_k(t_0+\tau)\mathrm{e}^{-\lambda_i\tau} d\tau \right\}, \tag{34}$$

where $p_k(t) = \Phi^T c(t)$.

Instead, the equation of the state space (31) for the *variances* reads:

$$\mathbf{A}\dot{\tilde{x}} - \mathbf{B}(t)\tilde{x} = e(t) \quad \text{where} \quad \tilde{x} = x - \widehat{x}, \tag{35}$$

with the relative characteristic equation

$$\mathbf{A}\Psi\Lambda - \mathbf{B}\Psi = 0. \tag{36}$$

Notice that the matrix $\mathbf{B}$ is time dependent, therefore, solving the eigenvalue problem (36) for large finite element systems may require a lot of computations, since the solution must be updated at every time step. Instead, we could recover the solution from the system (33), obtaining the eigenvectors Ψ from the matrices Φ and $H(t)$ (which is of course computed at every time step). In this way, using the transformation $\tilde{x} = \Psi\tilde{z}$ the Eq. (35) reads:

$$\mathbf{P}_z = E(z\dot{z}^T), \tag{37}$$

where the elements of the covariance matrix $\mathbf{P}_z$ are

$$P_{ij}(t) = \mathrm{e}^{(\lambda_i+\dot{\lambda}_j)(t-t_0)} \left\{ P_{ij}(t_0) + \int_0 (t-t_0) F_{ij} \mathrm{e}^{-(\lambda_i+\dot{\lambda_j})\tau} d\tau \right\}. \tag{38}$$

In the previous equation, F represents the autocorrelation matrix of the right hand side vector in modal coordinates i.e. $E\left\{\Psi^T e(t) e^T(t+\tau)\Psi\right\} = F\delta t$.

We can summarize the algorithm for calculating the response of the system in the following steps:

- Predict mean value with Eq. (34)
- Compute the matrix H
- Reconstruct the eigenvectors Ψ from Φ
- Predict the covariance matrix from (38)
- Transform the mean of the response from modal to physical coordinates
- Use $\mathbf{P}_x = \Psi\mathbf{P}_z\dot{\Psi}^T$ to obtain the covariance matrix in the real space

There is also another way to transform backward the covariance matrix. Considering the equation for the condtional mean of the state variable

$$\widehat{x}(t_{k+1} \mid t_{k+1}) = \widehat{x}(t_{k+1} \mid t_k) + \mathbf{G}(y(t_{k+1}) - \mathbf{T}\widehat{x}(t_{k+1} \mid t_k)), \tag{39}$$

with $\mathbf{G} = \mathbf{P}_x(t_{k+1} \mid t_k)\mathbf{T}^T \left\{\mathbf{T}\mathbf{P}_x(t_{k+1} \mid t_k)\mathbf{T}^T + \mathbf{N}\right\}^{-1}$ and $\mathbf{N}$ the noise covariance matrix.

After filtering we get the covariance matrix of the response, which reads

$$\mathbf{P}_x(t_{k+1} \mid t_{k+1}) = (\mathbf{I} - \mathbf{G}\mathbf{T})\mathbf{P}_x(t_{k+1} \mid t_k). \tag{40}$$

One of the drawbacks of the extended Kalman filtering is that it requires a priori knowledge of the mean and covariance matrix of the system response. Sometimes we can just guess the initial estimate of parameters, taking into account their relation with the root mean square value of the measured time series and choosing the one with less uncertainty. About the identification problem for actual material, also in order to consider different methodologies, it deserves to mention the review paper [61]

4.3 Sensitivity analysis

The most important problem when dealing with viscoelastic material is that, using differential model, one has to deal with a big number of constants, independent of frequency material parameter, in order to properly model the behaviour of the body, still considering the widest range of frequencies as possible. Therefore, may result difficult to identify which term have to be taken in consideration, which of them play an important role or, on the other hand, which of them has small effect and hence can be neglected. In our case, we consider mechanical models which are combinations of few springs and dashpots, from which we can get some useful information. But if we have to deal with more complex models made of a higher number of elements the investigation of their influence with respect to the associated parameter may become much harder. For this reason we can introduce a method made of optimization techniques and sensitivity analysis, which is able to recover the problem also in the case in which a wide number of unknown material parameters is encountered. In this section we are going to confront forced harmonical vibration tests made on Asphalt concrete with the previously described models for this material; from now on, all the variables with subscript e will denote experimentally obtained values. The laboratory measurements will provide informations about amplitude of the response and phase shift between it and the excitation, for a discrete frequency set ω_i covering a wide range of ω, for $i = 1, ..., N_e$, N_e denoting the number of experiments, within the material has to be considered.

Let us consider Eq. (19). For given haromonical motion with frequency ω_i we can write the complex stiffness as

$$E_i^*(\omega_i) = \frac{\sum_{k=0}^{N} q_k (i\omega_i)^k)}{\sum_{k=0}^{M} p_k (i\omega_i)^k)} = E_i^R + i E_i^I \tag{41}$$

whereas the amplitudes of stress and strain are

$$\sigma_i = \sqrt{(\sigma_i^R)^2 + (\sigma_i^I)^2}, \qquad \epsilon_i = \sqrt{(\epsilon_i^R)^2 + (\epsilon_i^I)^2}. \tag{42}$$

Once we have a set N_e of measurements and we know the components of the amplitudes of stresses $\sigma_{i,e}^R$, $\sigma_{i,e}^I$ and strains $\epsilon_{i,e}^R$, $\epsilon_{i,e}^I$, for different vibration frequencies ω_i, $i = 1, ..., N_e$ we can introduce an objective function J which we use for material parameters identification. We propose one which is an overall measure of the discrepancy between the calculated components of the stiffnesses ($E_{i,e}^R$, $E_{i,e}^I$, E_i^R, E_i^I) and the ones obtained by experimental measurements:

$$J = \sum_{i=1}^{N_e} \left[(E_i^R - E_{i,e}^R)^2 + (E_i^I - E_{i,e}^I)^2 \right], \tag{43}$$

where

$$E_i^R = \frac{A_1 B_1 + A_2 B_2}{B_1 B_1 + B_2 B_2}, \qquad E_i^I = \frac{A_2 B_1 - A_1 B_2}{B_1 B_1 + B_2 B_2} \tag{44}$$

resulting from Eq. (20), with

$$\begin{aligned} A_1 &= \sum_{k=0}^{N'-1} (-1)^k \omega_i^{2k} q_{2k}, \qquad A_2 = \sum_{k=1}^{N-N'+1} (-1)^{k-1} \omega_i^{2k-1} q_{2k-1} \\ B_1 &= \sum_{k=0}^{M'-1} (-1)^k \omega_i^{2k} p_{2k}, \qquad B_2 = \sum_{k=1}^{M-M'+1} (-1)^{k-1} \omega_i^{2k-1} p_{2k-1}. \end{aligned} \tag{45}$$

On the other hand, the experimental stiffness components are

$$E_{i,e}^R = \frac{\sigma_{i,e}^R \epsilon_{i,e}^R + \sigma_{i,e}^I \epsilon_{i,e}^I}{\epsilon_{i,e}}, \quad E_{i,e}^I = \frac{\sigma_{i,e}^I \epsilon_{i,e}^R + \sigma_{i,e}^R \epsilon_{i,e}^I}{\epsilon_{i,e}}. \tag{46}$$

Using all the previously stated relations, we can write the stationary condition for j, namely $\delta J = 0$, to find the optimal values for the parameters p_k and q_k:

$$\delta J = \sum_{k=0}^{M} \frac{\partial J}{\partial p_k} \delta p_k + \sum_{k=0}^{N} \frac{\partial J}{\partial q_k} \delta q_k = 0. \tag{47}$$

Now, we can analyse how sensitive is J to the parameters p_k and q_k, in order to understand and, whenever is necessary, to adapt their weight in the constitutive relations. After carrying out equations from (41) to (46), we can write the relations for sensitivity as follows:

$$\begin{aligned}
\delta_{p_k} J &= \frac{\partial J}{\partial p_k}\delta p_k = \left[2\frac{\partial E_i^R}{\partial p_k}\sum_{i=1}^{N_e}\left(E_i^R - E_{i,e}^R\right) + 2\frac{\partial E_i^I}{\partial p_k}\sum_{i=1}^{N_e}\left(E_i^I - E_{i,e}^I\right)\right]\delta p_k, \\
\delta_{q_k} J &= \frac{\partial J}{\partial q_k}\delta q_k = \left[2\frac{\partial E_i^R}{\partial q_k}\sum_{i=1}^{N_e}\left(E_i^R - E_{i,e}^R\right) + 2\frac{\partial E_i^I}{\partial q_k}\sum_{i=1}^{N_e}\left(E_i^I - E_{i,e}^I\right)\right]\delta q_k.
\end{aligned} \tag{48}$$

Finally we apply the next algorithm:

- Assume M and N arbitrarily, large enough
- Minimize the objective function to compute p_k and q_k
- Calculate the relative parameters values of the spring k_j and the damper c_j for the associated mechanical model to the assumed constitutive relation
- Estimate the individual components contribution to the mechanical model by means of sensitivity analysis and coefficients calculated in the previous step

  $$\delta_{k_j} J = \left[\sum_{k=0}^{M}\frac{\partial J}{\partial p_k}\frac{\partial p_k}{\partial k_j} + \sum_{k=0}^{N}\frac{\partial J}{\partial q_k}\frac{\partial q_k}{\partial k_j}\right]\delta k_j, \quad \delta_{c_j} J = \left[\sum_{k=0}^{M}\frac{\partial J}{\partial p_k}\frac{\partial p_k}{\partial c_j} + \sum_{k=0}^{N}\frac{\partial J}{\partial q_k}\frac{\partial q_k}{\partial c_j}\right]\delta c_j$$

  This gives an idea of which term may be neglected in the constitutive equation, still without loosing important information necessary for a good model of the material
- Obtain the constitutive equations from the simplified material model and eventually correct the parameters p_k and q_k repeating the minimization of the objective function.

In the next section we will see and discuss the results obtained by using the previous procedure, applied to the asphalt concrete model.

5 Results and comparison

In this section we show the results obtained by means of previously explained models and methods and compare them. At the end we try to choose which is the best model for each material, basically selecting the right number of parameters that are necessary to describe it.

We start with the Zener model, whose constants are obtained by the least square identification. As we already discussed, we will consider just two predominant modes of the solution, only one of which is then the most important. The spectral analysis of the beam response, recovered by B & K Dual Channel Analyzer 2032, confirm what theoretical analysis claims. Indeed, as we can see from Fig. 2, the first mode is like the one of the perfect elastic beam, damped very lightly, whereas the second mode is essential to estimate the damping constant. In Fig. 9 the results for the parameters of Zener model are shown.

We notice that the stiffness parameter p_0 converges almost ideally to the value $7.2 \cdot 10^7$ N/m^2, the damping constant p_1, even if not so smoothly, converges to $6.6 \cdot 10^5$ Ns/m^2, contrariwise, the time constant q_1 shows an oscillatory behaviour which does not approach to a specific value. Anyway we can estimate the parameter value around $8.0 \cdot 10^{-2}$ s, even if the variation are quite large.

Unfortunately, generally, the least square estimated give biased results and it needs noise free observations. What is more, very few statistical information about the estimated parameters is available. Even if we got very accurate results, thanks to the precise optical method, the resulted parameter value may contain bias errors due to uncertainty of the initial conditions (see for example [40]).

The results for the Voigt model, which we use with the Kalman filter, are shown in Figs. (10). We can see that, also in this case, the stiffness parameter converges quite quickly to the value $7.6 \cdot 10^7$ N/m^2. Notice that the obtained value is not very far from the one obtained with the Zener model. On the contrary the damping constant shows large fluctuation at the beginning, still converging to $5.4 \cdot 10^5$ Ns/m^2 after 120 time steps.

Let us consider the standard deviations of these values (Fig. 11): for the constant p_0 it reduces to 0 already after $30 - 40$ iterations, while for p_1 decreases much slower , and we need a quite large amount of time to identify the damping. The obtained value for this latter constant is considerably smaller (about 20%) than the one obtained for the Zener material

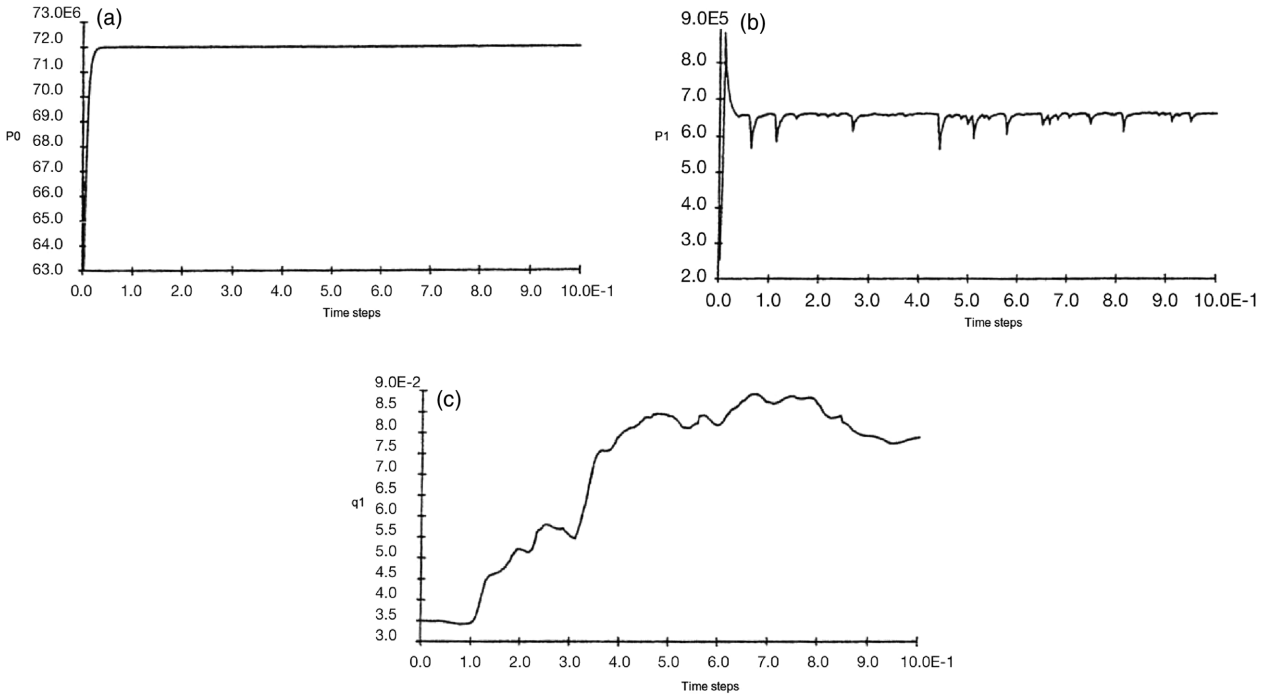

Fig. 9 Zener's model material parameters by means of least square estimation: a-stiffness constant p_0; b-damping constant p_1; c-time constant q_0.

model. We can thus conclude that the Voigt model is not capable of representing in a proper way the viscoelastic behaviour of the PVC beam, since it does not include the relaxation effect which we observed from the free vibration test (see Fig. 2.

Concerning the method explained for the Asphalt model, let us start with an initial guess of $M = 2$ and $N = 2$. We consider a series of frequencies for the vibrations $0.1\ \text{Hz} < f_i < 50.0\ \text{Hz}$, for which experimental datas are provided. The associated material model is the five-parameters model, shown in Fig. 12, for which

$$\begin{aligned} p_0 &= k_2(k_1 + k_3), & q_0 &= k_1 k_2 k_3, \\ p_1 &= c_2(k_1 + k_2 + k_3) + c_1 k_2, & q_1 &= k_3\left[c_2(k_1 + k_2) + c_1 k_2\right], \\ p_2 &= c_1 c_2, & q_2 &= k_3 c_1 c_2. \end{aligned} \tag{49}$$

We impose the additional constrain of $p_k \geqslant 0$ and $q_k \geqslant 0$, minimize the objective function (43) and find that for some sub-domain of $\omega\, q_0 = 0$ yielding $k_1 = 0$. Thus the complex five-parameters model is simplified to the Burgers model. In the Fig. 13, the results for complex stiffness modulus and phase shift are presented (in red) and compared to the experimental measurements and to the geometrical method, proposed in the latest fifties by Bland and Lee. As we can see, even if our theoretical results do not perfectly fit perfectly the experimental ones, they are significantly better than the ones obtained with the geometrical method. Indeed, Bland an Lee introduced that method specifically for viscoelastic materials which respond to Burgers model, while our method is more general and capable to better capture the material behaviour. Moreover, in order to check our sensitivity analysis, to understand which is the relevance of each parameter, as initial guess, we used different numbers of parameters, to perform the identification. The generalized model scheme is shown in Fig. 14. In order to identify the material parameter of the constitutive model, we minimized the following objective function

$$J = \sum_{i=1}^{N_e} \left[\left(\frac{E_i^* - E_{i,e}^*}{E_{min}^*}\right)^2 + \left(\frac{\delta_i - \delta_{i,e}}{\delta_{min}}\right)^2 \right], \tag{50}$$

where $E_i^* = \sqrt{(E_i^R)^2 + (E_i^I)^2}$, modulus of the complex stiffness, and δ_i is the phase shift introduced in Eq. (2). The results for coefficients computed for models with 4, 6, 8, and 10 parameters are reported in the Table 1.

From the Fig. 15-a, it can be observed that theoretical results for values of the complex stiffness fit sufficiently well to the experimental measured ones. We also noticed that the picture does not change when increasing, above 8, the number of components used in the material model, therefore they are not reported. On the other hand, if we observe the results for the phase shift, reported in Fig. 15-b, the previous assertion can not be repeated.

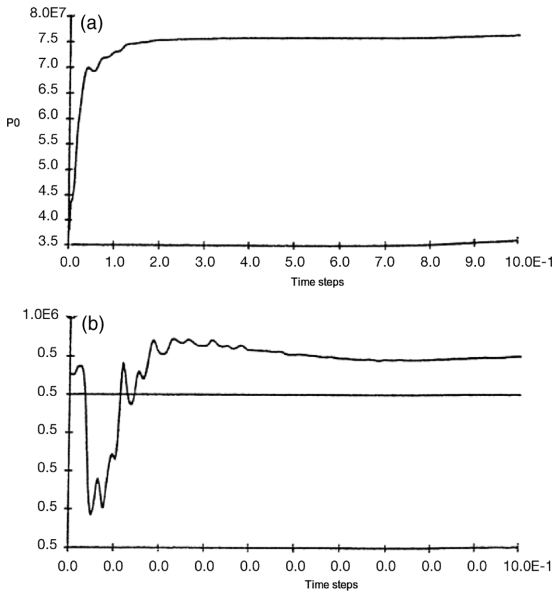

Fig. 10 Voigt's model material parameters by means of Kalman filtering: a-stiffness constant p_0; b-damping constant p_1.

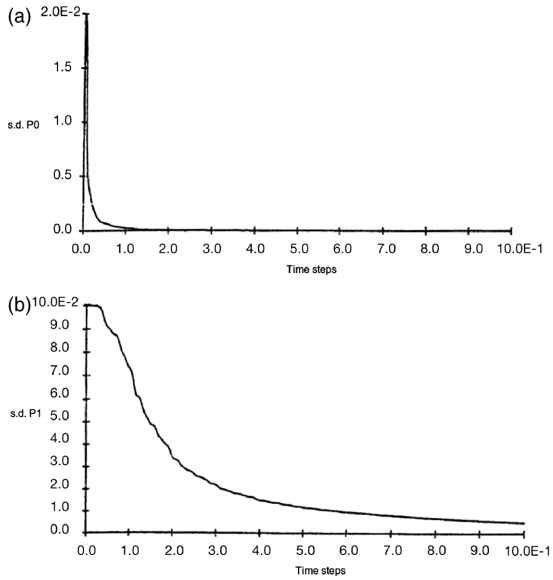

Fig. 11 Standard deviations of: a-stiffness constant p_0; b-damping constant p_1.

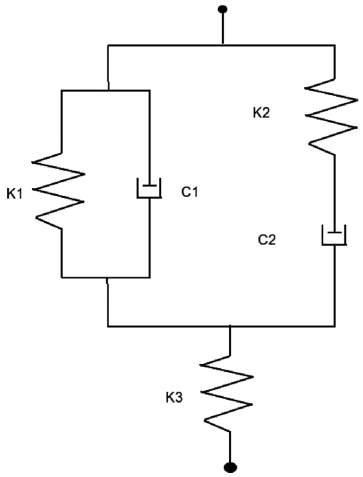

Fig. 12 Schematic representation of the five parameters material model.

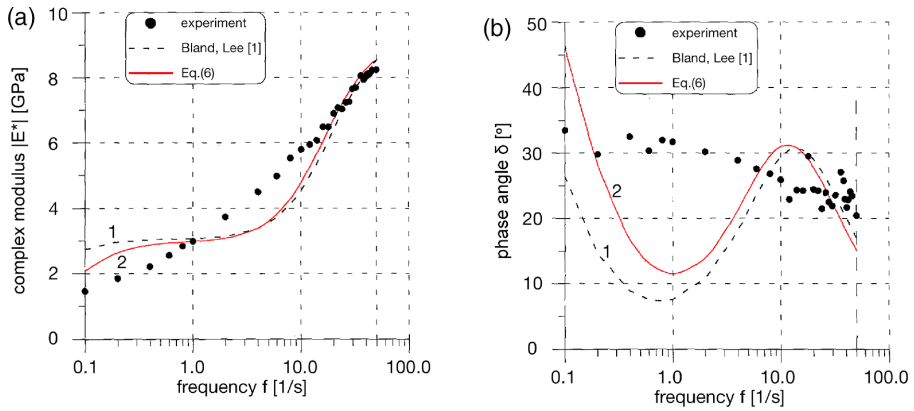

Fig. 13 a-Complex modulus, function of frequency; b-Phase shift, function of frequency.

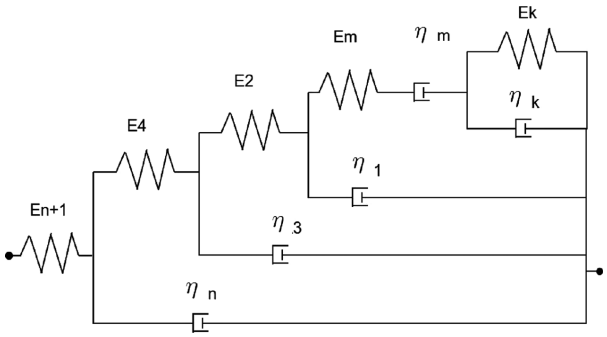

Fig. 14 Schematic representation of the general model for viscoelastic materials.

Table 1 Obtained coefficients computed for models with different number of parameters.

			4-par.	6-par.	8-par.	10-par.
1	E_k	GPa	4.4610	3.484613	3.484405	3.475803
2	η_k	GPa · s	0.1051	0.433184	0.871770	0.858180
3	E_M	GPa	9.1800	9.116613	7.335442	7.363758
4	η_M	GPa · s	4.613	4.590611	4.960377	4.956908
5	η_1	GPa · s		0.047036	0.183867	0.178332
6	E_2	GPa		13.43623	10.33714	16.79353
7	η_3	GPa · s			0.023758	0.002016
8	E_4	GPa			19.04319	23.01568
9	η_5	GPa · s				0.017757
10	E_M	GPa				23.76724

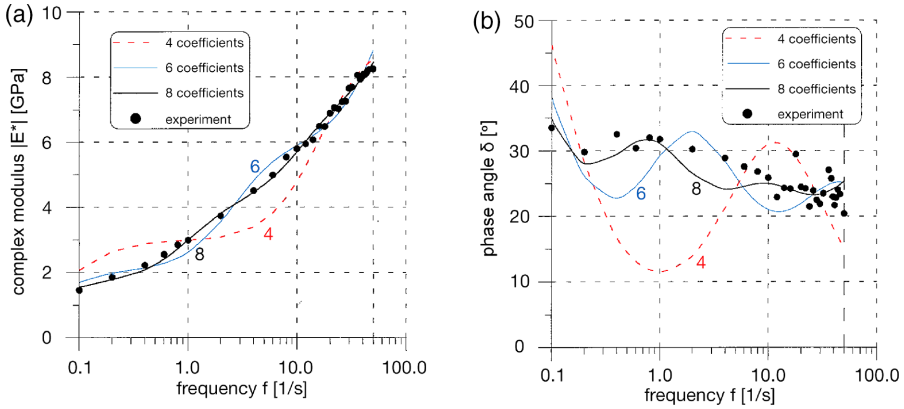

Fig. 15 a-Complex modulus, function of frequency; b-Phase shift, function of frequency.

This confirms the fact that, since the phase shift is a parameter which is easily affected in identification, may be exploited as a measure of the accuracy of any proposed material model.

Finally, we report how the sample responds to harmonical excitation, in time domain, compared to a 4-parameters and 8-parameters models, in the case of two different oscillation frequencies. We can observe that the biggest difference between theoretical and experimental results appear in the 4-parameters model (in red) and that, once again, we have good agreement in for E^*, even for low parameter model, while the phase shift differs significantly, even if it is still better fitted for higher parameter material model.

The generalization of the results here provided is of course of great interest. In particular, one may think to the following possibilities:

- Generalizing the method to two- and three-dimensional bodies; this may entail the need to address the problems arising from a more complex geometry of the specimens. From a numerical point of view, Finite Elements scheme with high regularity (as for instance isogeometric analysis [7,12,32]) may be useful in order to address these problems.
- Including in the beam model employed more general deformations (see e.g. [37,41–43])
- Considering other kinds of concrete with additional properties (see e.g. the concrete with enhanced dissipation properties studied in [54–56])
- Considering more general dependency of the energy on the kinematic descriptors, i.e. higher gradient models (see e.g. [1,4,6,15,16,18–22,27,33,38,57,59,62] for theoretical aspects and [14,17,45,50,52,53] for numerical results). This can be especially interesting if one wants to apply the methods described herein to objects produced by means of computer-aided manufacturing [23].
- Considering more general kinematical descriptors, i.e. microstructured continuum models (see e.g. [2, 3, 6, 44, 46–49, 58, 60, 63]).

6 Conclusions

If we want fully describe the mechanical characteristics of viscoelastic materials, nonlinear material model must be consider. However, if we just want to consider only selected properties of the materials, simplified viscoelastic constitutive relation may be useful, under certain loading conditions. This significantly restricts the field of applicability of the models, but ensures simplicity in implementation and understanding of them. This paper concerns the problem of modelling and identifying viscoelastic properties of PVC cantilever beam and Asphalt concrete by comparison with experimental measurements. Plastic effects were neglected, as well as temperature ones, and only viscoelastic properties were taken into consideration. We showed that even if the Voigt-Kelvin is applicable for the description of the viscoelastic beam and gives a good estimate for the stiffness, it gives significant errors for the damping parameter, while Maxwell-Zener three-parameter model is capable to better capture both the features of the material. Least square and Kalman filtering are both reliable methods for identification of stiffness, wile concerning the damping coefficient the second one works better if sufficiently large time interval is considered. Moreover, Kalman filter is able to speed up the iteration procedure, reduce the computational effort for multi degree of freedom systems and automatically filters the noise in measurements. The experimental measurement showed that one has to pay attention when using differential constitutive equations with constant coefficient, like the Burgers law, especially when a significant gamma of frequencies have to be considered, since the material coefficients may be strain velocity dependent. In the case of Asphalt concrete, we choose an objective function which measures the offset between the complex modulus of a real material and the one theoretically obtained when considering a specific material model. We showed that the phase shift plays a more important role than other parameters, in identification, since it represents a characteristic feature of the material. Moreover, it was observed that, increasing the number of the parameters in the material model, it is possible to get a improved description of the material, still keeping in mind that there exist a best number of material number, after which, adding complexity in the description is useless. Thus, in order to identify the ideal number of parameters to used, a sensitivity analysis was proposed and used.

We conclude reminding that the constant parameters contained in models obtained by comparison with specific experimental test, usually do not agree with those used in a model obtained on the basis of another. That is why, in order to improve the accuracy and the applicability of a model, one should take into account non constant material parameters.

References

[1] J. J. Alibert, P. Seppecher, and F. dell'Isola, Truss modular beams with deformation energy depending on higher displacement gradients, Math. Mech. Solids **8**(1), 51–73 (2003).

[2] H. Altenbach and V. A. Eremeyev, Analysis of the viscoelastic behavior of plates made of functionally graded materials, ZAMM-Journal of Applied Mathematics and Mechanics/Zeitschrift für Angewandte Mathematik und Mechanik **88**(5), 332–341 (2008).

[3] H. Altenbach and V. A. Eremeyev, On the linear theory of micropolar plates, ZAMM-Journal of Applied Mathematics and Mechanics/Zeitschrift für Angewandte Mathematik und Mechanik **89**(4), 242–256 (2009).

[4] N. Auffray, F. dell'Isola, V. Eremeyev, A. Madeo, and G. Rosi, Analytical continuum mechanics à la Hamilton–Piola least action principle for second gradient continua and capillary fluids, Math. Mech. Solids **20**(4), 375–417 (2015).

[5] A. Bilotta, G. Formica, and E. Turco, Performance of a high-continuity finite element in three-dimensional elasticity, International Journal for Numerical Methods in Biomedical Engineering **26**(9), 1155–1175 (2010).

[6] A. Carcaterra, F. dell'Isola, R. Esposito, and M. Pulvirenti, Macroscopic description of microscopically strongly inhomogenous systems: A mathematical basis for the synthesis of higher gradients metamaterials, Arch. Ration. Mech. Anal. **218**(3), 1239–1262 (2015).

[7] A. Cazzani, M. Malagù, and E. Turco, Isogeometric analysis: a powerful numerical tool for the elastic analysis of historical masonry arches, Contin. Mech. Thermodyn. 1–18 (2014).

[8] A. Cazzani, M. Malagù, and E. Turco, Isogeometric analysis: a powerful numerical tool for the elastic analysis of historical masonry arches, Contin. Mech. Thermodyn. **28**(1-2), 139–156 (2016).

[9] A. Cazzani, M. Malagù, E. Turco, and F. Stochino, Constitutive models for strongly curved beams in the frame of isogeometric analysis, Math. Mech. Solids **21**(2), 182–209 (2016).

[10] A. Cazzani, F. Stochino, and E. Turco, An analytical assessment of finite element and isogeometric analyses of the whole spectrum of Timoshenko beams, ZAMM-Journal of Applied Mathematics and Mechanics/Zeitschrift für Angewandte Mathematik und Mechanik **96**(10), 1220–1244 (2016).

[11] A. Cazzani, F. Stochino, and E. Turco, On the whole spectrum of Timoshenko beams. Part I: a theoretical revisitation, Zeitschrift für Angewandte Mathematik und Physik **67**(2), 1–30 (2016).

[12] J. A. Cottrell, T. J. Hughes, and Y. Bazilevs, Isogeometric Analysis: Toward Integration of CAD and FEA (John Wiley & Sons, 2009).

[13] M. Cuomo, L. Contrafatto, and L. Greco, A variational model based on isogeometric interpolation for the analysis of cracked bodies, Int. J. Eng. Sci. **80**, 173–188 (2014).

[14] A. Della Corte, A. Battista et al., Referential description of the evolution of a 2D swarm of robots interacting with the closer neighbors: perspectives of continuum modeling via higher gradient continua, Int. J. Non-Linear Mech. **80**, 209–220 (2016).

[15] F. dell'Isola, P. Seppecher, and A. Della Corte, The postulations à la D'Alembert and à la Cauchy for higher gradient continuum theories are equivalent: a review of existing results, Proc. R. Soc. A, **471**, 2183–2207 (2015).

[16] F. dell'Isola, U. Andreaus, and L. Placidi, At the origins and in the vanguard of peridynamics, non-local and higher-gradient continuum mechanics: An underestimated and still topical contribution of gabrio piola, Math. Mech. Solids **20**(8), 887–928 (2015).

[17] F. dell'Isola, M. d'Agostino, A. Madeo, P. Boisse, and D. Steigmann, Minimization of shear energy in two dimensional continua with two orthogonal families of inextensible fibers: The case of standard bias extension test, J. Elast. **122**(2), 131–155 (2016).

[18] F. dell'Isola, G. Sciarra, and S. Vidoli, Generalized Hooke's law for isotropic second gradient materials, Proceedings of the Royal Society of London A: Mathematical, Physical and Engineering Sciences **465**, 2177–2196 (2009).

[19] F. dell'Isola and P. Seppecher, The relationship between edge contact forces, double forces and interstitial working allowed by the principle of virtual power, Comptes Rendus de l Académie des Sciences-Series IIB-Mechanics-Physics-Astronomy **320**(5), 211–216 (1995).

[20] F. dell'Isola and P. Seppecher, Edge contact forces and quasi-balanced power, Meccanica **32**(1), 33–52 (1997).

[21] F. dell'Isola, P. Seppecher, and A. Madeo, How contact interactions may depend on the shape of Cauchy cuts in Nth gradient continua: approach 'à la D'Alembert', Z. Angew. Math. Phys. **63**(6), 1119–1141 (2012).

[22] F. dell'Isola and D. Steigmann, A two-dimensional gradient-elasticity theory for woven fabrics, J. Elast. **118**(1), 113–125 (2015).

[23] F. dell'Isola, D. Steigmann, and A. Della Corte, Synthesis of fibrous complex structures: Designing microstructure to deliver targeted macroscale response, Appl. Mech. Rev. **67**(6), 21 (2015).

[24] J. P. Den Hartog, Mechanical Vibrations (Courier Corporation, 1985).

[25] L. Dietrich and Z. L. Kowalewski, Experimental investigation of an anisotropy in copper subjected to predeformation due to constant and monotonic loadings, Int. J. Plast. **13**(1), 87–109 (1997).

[26] L. Dietrich, K. Turski, M. Waniewski, Z. Dziankowski, and R. Kiryk, Techniques for studying the mechanical properties of materials in complex stress states, NASA STI/Recon Technical Report N **95** (1994).

[27] M. Ferretti, A. Madeo, F. dell'Isola, and P. Boisse, Modeling the onset of shear boundary layers in fibrous composite reinforcements by second-gradient theory, Z. Angew. Math. Phys. **65**(3), 587–612 (2014).

[28] A. Galucio, J. F. Deü, and R. Ohayon, Finite element formulation of viscoelastic sandwich beams using fractional derivative operators, Computational Mechanics **33**(4), 282–291 (2004).

[29] L. Greco and M. Cuomo, B-Spline interpolation of Kirchhoff-Love space rods, Comput. Methods Appl. Mech. Eng. **256**, 251–269 (2013).

[30] L. Greco and M. Cuomo, An implicit G^1 multi patch B-spline interpolation for Kirchhoff-Love space rod, Comput. Methods Appl. Mech. Eng. **269**, 173–197 (2014).

[31] T. Herrmann and V. Chaika, Parameter identification of non-classically damped mechanical structures in time domain, Inverse Problems in Engineering **6**(2), 155–175 (1998).

[32] T. J. Hughes, J. A. Cottrell, and Y. Bazilevs, Isogeometric analysis: Cad, finite elements, nurbs, exact geometry and mesh refinement, Comput. Methods Appl. Mech. Eng. **194**(39), 4135–4195 (2005).

[33] A. Javili, F. dell'Isola, and P. Steinmann, Geometrically nonlinear higher-gradient elasticity with energetic boundaries, J. Mech. Phys. Solids **61**(12), 2381–2401 (2013).

[34] T. Lekszycki, Application of variational methods in analysis and synthesis of viscoelastic continuous systems, J. Struct. Mech. **19**(2), 163–192 (1991).

[35] T. Lekszycki, Optimal design of vibrating structures, Concurrent Engineering: Tools and Technologies for Mechanical System Design 767–785 (1993).

[36] T. Lekszycki, N. Olhoff, and J. J. Pedersen, Modelling and identification of viscoelastic properties of vibrating sandwich beams, Compos. Struct. **22**(1), 15–31 (1992).

[37] A. Luongo and D. Zulli, Mathematical Models of Beams and Cables (John Wiley & Sons, 2013).

[38] A. Madeo, L. Placidi, and G. Rosi, Towards the design of metamaterials with enhanced damage sensitivity: Second gradient porous materials, Res. Nondestruct. Eval. **25**(2), 99–124 (2014).
[39] F. Meral, T. Royston, and R. Magin, Fractional calculus in viscoelasticity: an experimental study, Commun. Nonlinear Sci. Numer. Simul. **15**(4), 939–945 (2010).
[40] H. Natke, Deliberations on the improvement of the computational model with measured eigenmagnitudes(for linear elastomechanic systems), Rev. Roum. Sci. Tech. Ser. Mec. Appl. **28**, 159–173 (1983).
[41] G. Piccardo, F. Tubino, and A. Luongo, A shear–shear torsional beam model for nonlinear aeroelastic analysis of tower buildings, Z. Angew. Math. Phys. **66**(4), 1895–1913 (2015).
[42] G. Piccardo, G. Ranzi, and A. Luongo, A complete dynamic approach to the Generalized Beam Theory cross-section analysis including extension and shear modes, Math. Mech. Solids **19**(8), 900–924 (2014).
[43] G. Piccardo, G. Ranzi, and A. Luongo, A direct approach for the evaluation of the conventional modes within the GBT formulation, Thin-Walled Struct. **74**, 133–145 (2014).
[44] W. Pietraszkiewicz and V. Eremeyev, On natural strain measures of the non-linear micropolar continuum, Int. J. Solids Struct. **46**(3), 774–787 (2009).
[45] L. Placidi, U. Andreaus, A. Della Corte, and T. Lekszycki, Gedanken experiments for the determination of two-dimensional linear second gradient elasticity coefficients, Z. Angew. Math. Phys. **66**(6), 3699–3725 (2015).
[46] L. Placidi, S. H. Faria, and K. Hutter, On the role of grain growth, recrystallization and polygonization in a continuum theory for anisotropic ice sheets, Ann. Glaciol. **39**(1), 49–52 (2004).
[47] L. Placidi, R. Greve, H. Seddik, and S. H. Faria, Continuum-mechanical, Anisotropic Flow model for polar ice masses, based on an anisotropic Flow Enhancement factor, Contin. Mech. Thermodyn. **22**(3), 221–237 (2010).
[48] L. Placidi and K. Hutter, An anisotropic flow law for incompressible polycrystalline materials, Z. Angew. Math. Phys. ZAMP **57**(1), 160–181 (2005).
[49] L. Placidi and K. Hutter, Thermodynamics of polycrystalline materials treated by the theory of mixtures with continuous diversity, Contin. Mech. Thermodyn. **17**(6), 409–451 (2006).
[50] L. Placidi, G. Rosi, I. Giorgio, and A. Madeo, Reflection and transmission of plane waves at surfaces carrying material properties and embedded in second-gradient materials, Math. Mech. Solids **19**(5), 555–578 (2013).
[51] B. Ranlecki, L. Dietrich, Z. Kowalewski, G. Socha, S. Miyazaki, K. Tanaka, and A. Ziółkowski, Experimental methodology for tini shape memory alloy testing under complex stress state, Arch. Mech. **51**(6), 727–744 (1999).
[52] A. Rinaldi and L. Placidi, A microscale second gradient approximation of the damage parameter of quasi-brittle heterogeneous lattices, ZAMM-Journal of Applied Mathematics and Mechanics/Zeitschrift für Angewandte Mathematik und Mechanik **94**(10), 862–877 (2014).
[53] G. Rosi, I. Giorgio, and V. A. Eremeyev, Propagation of linear compression waves through plane interfacial layers and mass adsorption in second gradient fluids, ZAMM-Journal of Applied Mathematics and Mechanics/Zeitschrift für Angewandte Mathematik und Mechanik **93**(12), 914–927 (2013).
[54] D. Scerrato, I. Giorgio, A. Della Corte, A. Madeo, N. Dowling, and F. Darve, Towards the design of an enriched concrete with enhanced dissipation performances, Cement and Concrete Research **84**, 48–61 (2016).
[55] D. Scerrato, I. Giorgio, A. Della Corte, A. Madeo, and A. Limam, A micro-structural model for dissipation phenomena in the concrete, Int. J. Numer. Anal. Methods Geomech. **39**(18), 2037–2052 (2015).
[56] D. Scerrato, I. Giorgio, A. Madeo, A. Limam, and F. Darve, A simple non-linear model for internal friction in modified concrete, Int. J. Eng. Sci. **80**, 136–152 (2014).
[57] G. Sciarra, F. dell'Isola, and O. Coussy, Second gradient poromechanics, Int. J. Solids Struct. **44**(20), 6607–6629 (2007).
[58] H. Seddik, R. Greve, L. Placidi, I. Hamann, and O. Gagliardini, Application of a continuum-mechanical model for the flow of anisotropic polar ice to the EDML core, Antarctica, Journal of Glaciology **54**(187), 631–642 (2008).
[59] P. Seppecher, J. J. Alibert, and F. dell'Isola, Linear elastic trusses leading to continua with exotic mechanical interactions, in: Journal of Physics: Conference Series, p. 012018 (2011).
[60] R. Serpieri, A. Della Corte, F. Travascio, and L. Rosati, Variational theories of two-phase continuum poroelastic mixtures: a short survey, in: Generalized Continua as Models for Classical and Advanced Materials (Springer, 2016), pp. 377–394.
[61] E. Turco, Tools for the numerical solution of inverse problems in structural mechanics: review and research perspectives, European Journal of Environmental and Civil Engineering 1–46 (2016).
[62] Y. Yang and A. Misra, Higher-order stress-strain theory for damage modeling implemented in an element-free Galerkin formulation, CMES-Computer Modeling in Engineering & Sciences **64**(1), 1–36 (2010).
[63] Y. Yang and A. Misra, Micromechanics based second gradient continuum theory for shear band modeling in cohesive granular materials following damage elasticity, Int. J. Solids Struct. **49**(18), 2500–2514 (2012).